



Copper Deposition onto Silicon by Galvanic Displacement: Effect of Silicon Dissolution Rate

Calvin P. daRosa,* Roya Maboudian,**^z and Enrique Iglesia^z

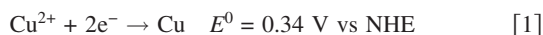
Department of Chemical Engineering, University of California, Berkeley, Berkeley, California 94720, USA

The rates of Cu deposition onto rotating Si electrodes were measured to probe the effects of mass transfer, Cu²⁺ reduction, and Si oxidation and dissolution on deposition dynamics. Cu deposition rates were proportional to CuSO₄ concentration and limited by Cu²⁺ diffusion and subsequent reduction at high HF concentrations ([HF]/[CuSO₄] > 20). In contrast, Si dissolution limited film growth at low HF concentrations ([HF]/[CuSO₄] < 10), and HF₂⁻ was identified as the most active Si etchant. The observed effects of rotation rate indicate that mass transfer of Cu²⁺ limits deposition rates, but mass transfer of HF does not. Open-circuit potential measurements and mixed-potential theory were used to develop a reaction-transport model that accurately predicts deposition rates over a broad range of Cu and HF concentrations. The structure of the films formed was probed by atomic force microscopy. The roughness of the Cu films decreased with increasing [HF]/[CuSO₄] ratios, as Si surfaces became less oxidized, and lateral connectivity between Cu nuclei increased.

© 2008 The Electrochemical Society. [DOI: 10.1149/1.2907155] All rights reserved.

Manuscript submitted November 28, 2007; revised manuscript received February 15, 2008.
Available electronically April 28, 2008.

Galvanic displacement has been used for metal deposition on Si for applications including microelectromechanical system,^{1,2} surface-enhanced Raman spectroscopy,³⁻⁵ and catalysis.^{6,7} Galvanic displacement offers the advantage of selective deposition because reduction of metal ions is coupled with oxidation and dissolution of the substrate. A schematic diagram of galvanic displacement of Cu onto Si is shown in Fig. 1, indicating the mass transfer and kinetic processes required for deposition. Fluoride species, HF in this case, must be added to dissolve oxidized Si and expose additional Si to continue galvanic displacement. Galvanic displacement occurs spontaneously when the depositing metal is more noble (easier to reduce) than both the substrate and hydrogen. Thus, Cu can be deposited by galvanic displacement because of its favorable reduction potential⁸



where NHE is the potential of the normal hydrogen electrode. Si is easily oxidized (Si²⁺/Si $E^0 = -0.81 \text{ V}^9$), making it a suitable substrate for galvanic displacement. In this work, the concentrations of Cu²⁺ and HF are varied to determine the effects of the oxidation and reduction half-reactions on Cu deposition rates and the structure Cu films.

Several studies have examined the effects of Cu²⁺ concentration on galvanic displacement rates. Deposition rates were found to be first-order in Cu²⁺ concentration for deposition on substrates including Si, Fe, and Zn.¹⁰⁻¹⁴ Less is known about the effect of HF concentration on deposition rates. Deposition rates increased with increasing HF concentration for deposition of Cu and Ag on Si, but few HF concentrations were studied, and the relationship between HF concentration and Cu deposition rates was not quantified.^{10,15} In this work, we investigate the effect of Si dissolution on Cu deposition rates by systematically varying the HF concentration.

In addition to the effects of formal HF concentration, the fluoride species responsible for Si dissolution were also probed. Dissolution via parallel pathways involving HF and HF₂⁻ has been proposed,¹⁶⁻¹⁸ and recent work has supported this mechanism for electroless "stain etching" of Si with various oxidants.^{19,20} In contrast, the rate of AuCN reduction during galvanic displacement was reported to increase as [HF]^{0.5}, independent of [HF₂⁻], during Au nanocluster deposition on Si.²¹ In this work, the Si etchant was identified by adding HNO₃ and KOH to alter the solution pH and independently change the relative concentrations of fluoride species present at equilibrium.

Further understanding of the deposition mechanism can also be used to tailor deposition conditions to produce films with the desired properties. Previous studies have noted higher Cu nucleation rates on Si with increasing HF concentrations.²² Little has been reported, however, on the effects of HF concentration on the morphology of thicker (> 100 nm) films. Yang and Griffiths reported the formation of Ag clusters on oxidized Ge, and continuous films on reduced Ge.²³ The tendency to form isolated particles on oxidized substrates has also been shown for Ni nucleation on Si in the absence of HF.²⁴ Here, we use atomic force microscopy (AFM) to determine the effects of HF concentration on Cu morphology.

Experimental

The methods used in this work have been described previously.²⁵ Briefly, Cu was deposited onto rotating Si wafers ($\rho = 10\text{--}20 \text{ } \Omega \text{ cm}$, Wafernet) attached to the end of a rotating shaft (model A5R2, Pine Instruments). Rotating speeds were varied between 10 and 250 rad s⁻¹ (~100 to 2500 rpm), and deposition times between 10 and 900 s. Aqueous solutions of CuSO₄·5H₂O (0.0010–0.040 M, 99.3%, Fisher) and HF (0.010–1.0 M, 48%, EMD) were used for Cu deposition. The effect of HF speciation on deposition rates was probed by adding KOH (0–0.2 M, EMD, 85%) and HNO₃ (0–0.1 M, Fisher, 69%) to modify solution pH. Open-circuit potential (OCP) values were measured using a high-impedance voltmeter (Keithley 2400 SourceMeter) at a 14 Hz sampling rate, and data were recorded using LabTracer 2.0 software. Hg/Hg₂SO₄ was used as the reference electrode (REF621, Radiometer Analytical).

Cu surface structures were studied by AFM using a Digital Instruments Multimode III system in tapping mode. Film thicknesses were also determined by AFM by scratching the Cu film with Teflon

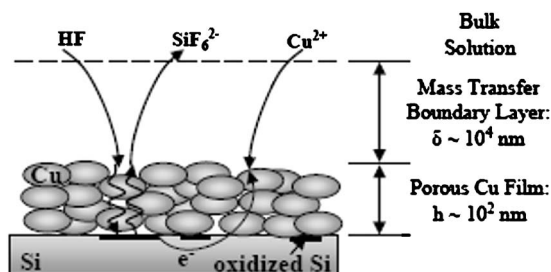


Figure 1. Model for Cu deposition on Si by galvanic displacement. Deposition involves mass transfer through a hydrodynamic boundary layer and a porous Cu film. Si oxidation, Cu²⁺ reduction, and dissolution of oxidized Si products at surfaces.

* Electrochemical Society Student Member.

** Electrochemical Society Active Member.

^z E-mail: maboudia@berkeley.edu; iglesias@berkeley.edu

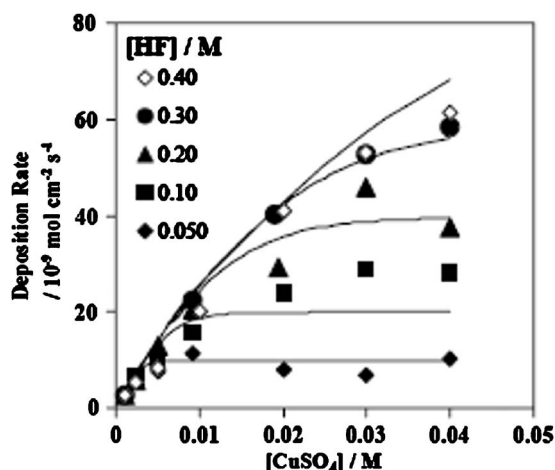


Figure 2. Dependence of Cu deposition rate on solution composition. The solid lines are deposition rates predicted by setting the Cu reduction and Si oxidation rates in Eq. 8 and 11 equal to each other using mixed-potential theory. Angular velocity = 50 s^{-1} , film thickness = 100 nm.

tweezers to expose the underlying Si and measuring the height differences between the Cu and Si surfaces. Deposition rates reported below were found by dividing the film thickness by the deposition time and assuming a void fraction of 0.15, as found previously.²⁵ The amounts of Cu deposited and of Si dissolved were also determined directly from UV-visible spectra of the contacting solution (Cary 400 Spectrometer).

Results and Discussion

Effect of silicon dissolution on copper deposition rates.— The effect of Si dissolution on Cu deposition rates was determined by varying the concentrations of both CuSO_4 and HF. Deposition rates for rotational angular velocities of 50 s^{-1} are shown in Fig. 2; the trends observed here are representative of those measured at other angular velocities (10 – 250 s^{-1}). For $[\text{HF}] \geq 0.30 \text{ M}$, Cu deposition rates were independent of $[\text{HF}]$, indicating that Si dissolution does not limit Cu deposition rates for the compositions studied. Cu deposition rates were first order in $[\text{CuSO}_4]$ (up to 0.030 M) for these high HF concentrations (Fig. 2), consistent with previous measurements of first-order Cu deposition kinetics in galvanic displacement.^{11,26,27} In more dilute HF solutions, however, deposition rates no longer increased linearly with increasing $[\text{CuSO}_4]$, reaching maximum constant values at high CuSO_4 concentrations. The deposition rates at these plateaus increased with increasing $[\text{HF}]$, suggesting that Si dissolution limits deposition rates under these conditions.

Si dissolution rates are coupled to Cu^{2+} reduction rates because the electrons consumed during Cu^{2+} reduction are supplied by Si oxidation, as depicted in Fig. 1. UV-visible spectra of deposition solutions revealed that the ratio of Cu deposited to Si dissolved was ~ 1 for high $[\text{HF}]/[\text{CuSO}_4]$ ratios (Table I). This indicates dissolution of Si as Si^{2+} was the primary Si oxidation pathway, as was observed previously for Cu galvanic displacement in 3.0 M HF .²⁵ In contrast, Cu:Si ratios increase and approach the value of 2 for $[\text{HF}]/[\text{CuSO}_4] < 10$, suggesting Si dissolution as Si^{4+} also occurs under these conditions, when Si dissolution limits Cu deposition rates. The transition from Si dissolution as Si^{2+} to Si^{4+} with decreasing $[\text{HF}]$ is consistent with previous results for Si oxidation and dissolution, which found that Si dissolved as Si^{4+} when the driving force for Si dissolution decreased relative to that for Si oxidation.²⁸

The limiting rates of Cu deposition depicted in Fig. 2 are consistent with limiting Si dissolution rates for the given HF concentrations. The maximum rates of oxidation and dissolution of Si rotating disk electrodes (RDEs) have previously been reported for a range of

Table I. Effect of solution composition on ratio of Cu deposited to Si dissolved measured from UV-visible spectra of deposition solutions. Cu:Si ratios increase as $[\text{HF}]/[\text{CuSO}_4]$ decreases, suggesting dissolution of Si as Si^{4+} occurs when Si dissolution limits deposition rates. $\omega = 50 \text{ s}^{-1}$.

[HF] (M)	[CuSO ₄] (M)	[HF]/[CuSO ₄]	Cu:Si (± 0.2)
0.10	0.0025	40	0.90
0.20	0.0050	40	0.75
0.050	0.0025	10	0.75
0.10	0.010	10	1.0
0.15	0.030	5	1.9
0.050	0.010	5	2.0
0.10	0.040	2.5	1.7

solution compositions and rotation speeds.^{29–31} The maximum Si^{2+} dissolution rates calculated from these data are slightly lower than the maximum rates of Cu deposition measured at these HF concentrations (Table II). Deposition rates exceeding the maximum rates of Si^{2+} dissolution also suggest that dissolution of Si as Si^{4+} occurs when Si dissolution limits Cu deposition rates, because the maximum rate of Si^{4+} is greater than that of Si^{2+} .^{28,29} This is consistent with Cu:Si stoichiometries reported in Table I. Si oxidation and dissolution rates during galvanic displacement are more than one order of magnitude greater than dissolution rates of bulk SiO_2 at similar HF concentrations.^{16,32,33} The higher rates found in this study may reflect higher mass transfer rates due to deposition on rotating samples or the presence of less dense oxide structures, which dissolve more quickly.³³

The deposition rate plateaus observed in Fig. 2 appeared at higher CuSO_4 concentrations as the HF concentration increased, suggesting that the rate-limiting step is determined by the relative concentrations of CuSO_4 and HF. Deposition rates were independent of HF concentration and limited by only Cu^{2+} reduction at high $[\text{HF}]/[\text{CuSO}_4]$ ratios (> 10), while Si dissolution rates also influenced Cu film growth at lower $[\text{HF}]/[\text{CuSO}_4]$ ratios. These findings are consistent with previous studies of the deposition of Pt onto Si, for which deposition rates increased with increasing $[\text{HF}]$ for $[\text{HF}]/[\text{H}_2\text{PtCl}_6]$ below ~ 12 , but became independent of $[\text{HF}]$ at higher $[\text{HF}]/[\text{H}_2\text{PtCl}_6]$ ratios.³⁴ As we show later, this ratio, and thus the identity of the rate-limiting reaction, also influences the morphology of the Cu films deposited.

Effect of pH and HF speciation on deposition rates.— The above results demonstrate the influence of Si dissolution on Cu deposition rates, but they cannot identify the fluoride species responsible for dissolving Si because the equilibrium concentrations of all fluoride species are strongly correlated with one another. HF is a weak acid that dissociates into H^+ and F^- .³⁵

Table II. Comparison of Cu deposition rates at high- $[\text{CuSO}_4]$ plateaus with maximum Si^{2+} dissolution rates reported previously for these HF concentrations and $\omega = 50 \text{ s}^{-1}$.

[HF] (per M)	Maximum Cu deposition rate (per $10^{-9} \text{ mol cm}^{-2} \text{ s}^{-1}$)	Maximum Si^{2+} dissolution rate ^a (per $10^{-9} \text{ mol cm}^{-2} \text{ s}^{-1}$)
0.050	8.0	6.2
0.10	24	15
0.20	40	36
0.30	60	59

^a Calculated from published data on effects of $[\text{HF}]$ and rotation speed on Si^{2+} dissolution rates.^{28,29}

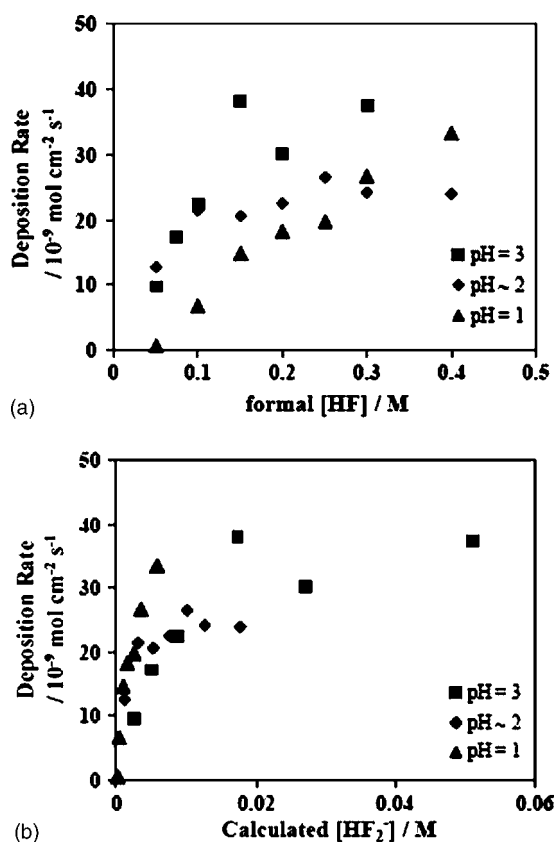
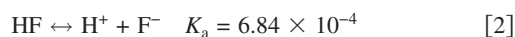
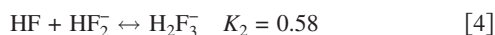
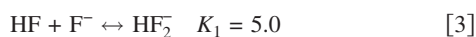


Figure 3. Effect of solution pH on Cu deposition rates. pH values were adjusted to 1 by adding 0.1 M HNO_3 and to 3 by adding the appropriate amount of KOH , as determined by the equilibria in Eq. 2-4. Activities of HF_2^- were determined from Eq. 2-4. $[\text{CuSO}_4] = 0.01$ M, $\omega = 50$ s^{-1} .



HF and F^- can react further to form HF_2^- and H_2F_3^- via the following reactions^{35,36}



Kolasinski used experimental results for HF speciation at equilibrium to determine the equilibrium constants listed above and to calculate the activity coefficients of HF and of charged species as functions of ionic strength.³⁵ These results were used to determine HF speciation in solutions used for Cu deposition, including the effects of CuSO_4 on ionic strength and $\text{SO}_4^{2-}/\text{HSO}_4^-$ acid-base equilibrium. The effect of equilibrium HF speciation on Cu deposition rates was then analyzed to determine the active species for Si dissolution.

HNO_3 and KOH were added to Cu deposition solutions to alter the pH and allow independent control of the total fluorine concentration and of the activity of each fluorine-containing component. Solution pH values were ~ 2 when no HNO_3 or KOH is added, and deposition rates in these solutions increase with increasing $[\text{HF}]$, as shown in Fig. 3a. Deposition rates were very low in dilute HF solutions ($[\text{HF}] \leq 0.1$ M) when HNO_3 was added to decrease the pH to a value of 1 (Fig. 3a). These low deposition rates indicate that HF itself is not solely responsible for Si dissolution because undissociated HF is the predominant fluorine species at pH 1. Very low galvanic displacement rates were observed previously when H_2SO_4 was added to solutions containing HF and CuSO_4 to decrease the pH below 0.4, but the authors did not provide an interpretation for these trends.³⁷ In contrast, deposition rates increased when KOH was added to increase the pH to 3 (Fig. 3a). The extent of HF dissociation

(Eq. 2) increases with increasing pH, as more F^- is formed to compensate for lower H^+ concentrations. This higher F^- concentration in turn increases the concentrations of HF_2^- and H_2F_3^- present at equilibrium (Eq. 3 and 4).

Cu deposition rates shown in Fig. 3a were compared to the calculated activity for each fluorine-containing component to determine the most active species for Si dissolution. Deposition rates were found to correlate most closely with the HF_2^- activity (Fig. 3b), suggesting HF_2^- is primarily responsible for Si dissolution. Cu deposition rates were strongly correlated with HF_2^- concentrations for CuSO_4 concentrations between 0.0025 and 0.030 M and initial HF concentrations between 0.025 and 1.0 M, further demonstrating the importance of this species for Si dissolution. Maximum HF_2^- concentrations were previously reported near pH 3, consistent with the increased rates we observe at this pH.²⁹ Our attempts to measure deposition rates at even higher pH values were unsuccessful because of the low solubility of $\text{Cu}(\text{OH})_2$ ($K_{\text{sp}} = 2.2 \times 10^{-20}$).³⁸

The proposed role of HF_2^- in Si dissolution is consistent with previous studies, which identified this species as the most active etchant of SiO_2 ^{16,32} and Si ^{17,18} in the absence of metal deposition. These authors proposed parallel dissolution pathways by HF and HF_2^- , and dissolution rate constants calculated for HF_2^- were 4–20 times larger than those for HF.^{16,17,29} Undissociated HF still contributes to Si dissolution despite lower rate constants because its equilibrium concentration is ~ 10 times greater than that of HF_2^- . Parallel dissolution by undissociated HF may explain why deposition rates in Fig. 3b are highest at a pH of 1 for a given HF_2^- activity: these solutions have higher concentrations of undissociated HF, which also dissolves oxidized Si. Rate constants for dissolution by HF and HF_2^- were estimated by assuming Cu deposition rates in dilute fluoride solutions (where deposition rates increase with increasing $[\text{HF}]$) equal the maximum rate of Si dissolution

$$r = k_{\text{HF}_2^-}(\text{HF}_2^-) + k_{\text{HF}}(\text{HF}) \quad [5]$$

The rate constant for Si dissolution by HF_2^- , $k_{\text{HF}_2^-}$, was found to be $(3.3 \pm 0.3) \times 10^{-3}$ cm s^{-1} , and k_{HF} is $(7 \pm 1) \times 10^{-5}$ cm s^{-1} . This low rate constant for Si dissolution by undissociated HF is consistent with lower Cu deposition rates at pH 1, when HF is the predominant F-containing species. The ratio of $k_{\text{HF}_2^-}$ to k_{HF} indicates that HF_2^- dissolves oxidized Si ~ 40 times faster than HF, which is somewhat higher than the reactivity ratio of 4–20 reported previously.^{16,17}

Effect of mass transfer on Cu deposition rates.— Si rotation speeds were varied to determine the contributions of boundary layer mass transfer and reaction kinetics to the Cu deposition rates reported above. Mass transfer rates to RDEs are proportional to $\omega^{1/2}$, as given by the Levich equation³⁹

$$k_m = 0.62\nu^{-1/6}D^{2/3}\omega^{1/2} \quad [6]$$

where ν is the solution kinematic viscosity, D is the diffusion coefficient of the species of interest, and ω is the angular rotation rate. If the reaction mechanism consists of boundary layer mass transfer followed by first-order chemical reaction at the solid surface, then the inverse deposition rate will equal the sum of these two resistances⁸

$$\frac{1}{r} = \frac{1}{kC} + \frac{\nu^{1/6}}{0.62D^{2/3}C\omega^{1/2}} \quad [7]$$

In this expression, k is the kinetic rate constant, C is the concentration of the rate-limiting reactant, and the other variables are as defined above. Equation 7 assumes that either the Cu reduction or the Si oxidation half reaction limits the deposition rate, and that its rate can be described by sequential boundary layer mass transfer and first-order chemical reactions. This is somewhat oversimplified because the driving forces for both half reactions affect deposition rates, as shown above (Fig. 1). Nevertheless, Eq. 7 provides insights

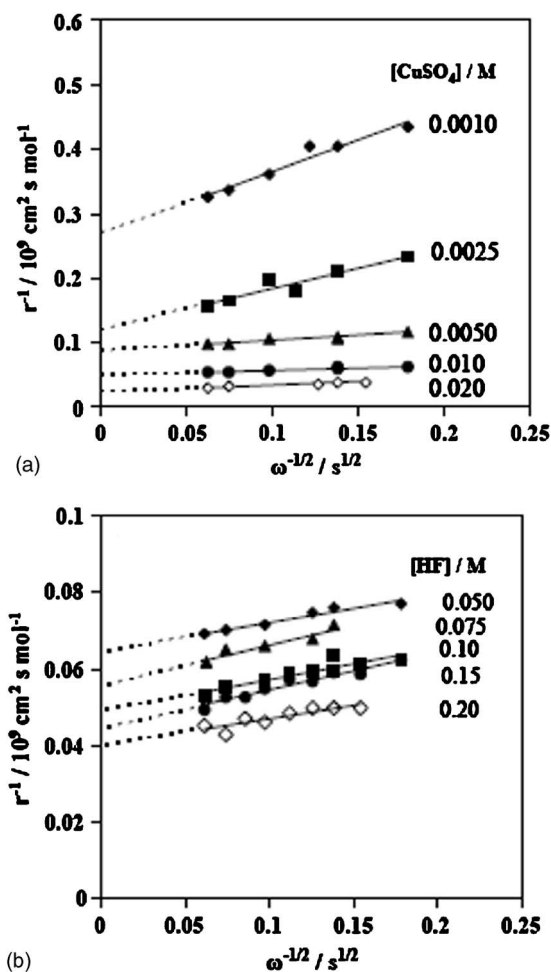


Figure 4. Effect of rotating speed (boundary layer mass transfer coefficient) on Cu deposition rates. Plots of r^{-1} vs $\omega^{-1/2}$ should be linear, with both the slope and the intercept inversely proportional to the activity of the diffusion-limited species, according to the Koutecky–Levich equation (Eq. 7): (a) Dependence of mass transfer and kinetic rates on CuSO_4 concentration. $[\text{HF}] = 0.10 \text{ M}$. Film thickness = 100 nm. (b) Dependence of mass transfer and kinetic rates on HF concentration. $[\text{CuSO}_4] = 0.010 \text{ M}$. Film thickness = 100 nm.

into the extent to which mass transfer limits deposition rates and into the identity of the diffusion-limited species. Equation 7 predicts that r^{-1} would increase linearly with $\omega^{-1/2}$ and that the consequent slope and intercept with the ordinate are inversely proportional to the concentration of whichever reactant limits measured rates.

Figure 4 shows the effects of rotation angular velocity and of solution composition on deposition rates. Inverse rates (r^{-1}) increased linearly with $\omega^{-1/2}$, which is consistent with predictions based on the Koutecky–Levich equation (Eq. 7) and suggests the deposition process is described accurately by the assumption of boundary layer mass transfer and first-order surface chemical reaction in series. Both the slope and the intercept decreased as CuSO_4 concentrations increased at a given HF concentration (Fig. 4a). Figure 5a shows that these values are nearly inversely proportional to CuSO_4 concentration, as predicted from Eq. 7 for deposition rates limited by Cu^{2+} mass transfer and reduction in series.

The influence of HF concentration on deposition rates is different from that of Cu^{2+} concentration. Consistent with Eq. 7, intercepts of the Koutecky–Levich plots shift to lower values as the concentration of HF increases (Fig. 4b), but these are not inversely proportional to $[\text{HF}]$ (Fig. 5b). In contrast, the slopes of the Koutecky–Levich plots, and thus the mass transfer rates of the diffusion-limited species,

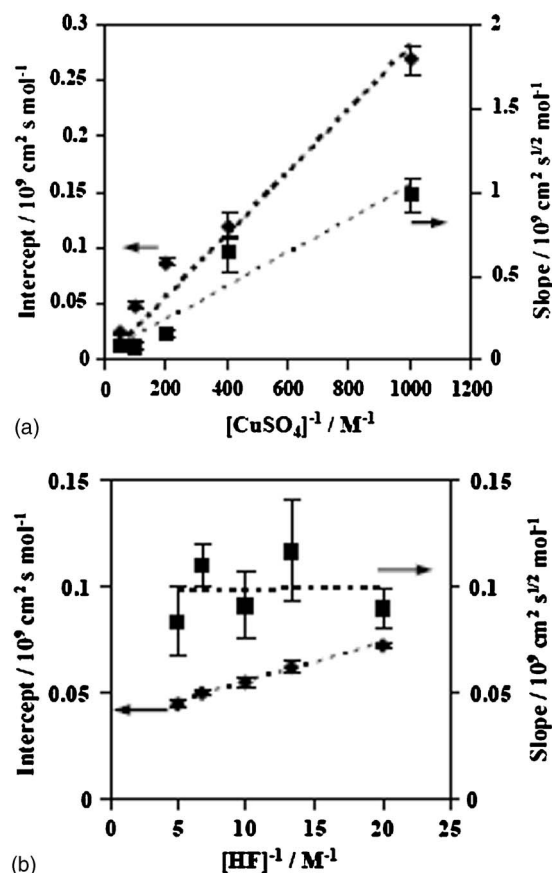


Figure 5. Best-fit values for the intercept (■) and the slope (◆) of the Koutecky–Levich plots in Fig. 4. According to the Koutecky–Levich equation (Eq. 7), the intercept represents the resistance to reaction kinetics, and the slope represents resistance to mass transfer: (a) Effect of CuSO_4 concentration on slope and intercept. Data are taken from Fig. 4a. (b) Effects of HF concentration on slope and intercept. Data are taken from Fig. 4b.

were unaffected by HF concentration when CuSO_4 concentration was held constant. This indicates that mass transfer of fluoride species did not limit deposition rates for the range of solution compositions studied here. This demonstrates that the effect of Si dissolution rates on Cu deposition rates (Fig. 2) is due solely to the kinetics of Si dissolution and not to mass transfer of fluoride species to the electrode surface. The effects of the individual half reactions are studied later in more detail, and the combined effects of reduction and dissolution are explored via the OCP.

Analysis of OCP during deposition.— OCP values were measured to determine the extent to which the oxidation and reduction half reactions limit measured rates and to elucidate the rate-limiting processes in each half reaction. The effects of CuSO_4 concentration on the time evolution of OCP values during deposition in 0.10 M HF are shown in Fig. 6. OCP values became more positive as CuSO_4 concentration increased, consistent with previous results showing that OCP values increased as the driving force for reduction increased.^{40,41} A maximum OCP value was observed at short times ($< 20 \text{ s}$) for all concentrations, and this maximum occurred at times inversely proportional to CuSO_4 concentration. These results suggest that the same amount of Cu has been deposited at each of these maxima. This hypothesis was also supported by experiments performed at different rotating speeds, which found that the times required to reach these maximum OCP values were inversely proportional to the Cu^{2+} mass transfer coefficient. Thus, a constant amount of Cu, corresponding to a film thickness of $\sim 10 \text{ nm}$, is deposited by the time the maximum OCP value is reached. This thickness may

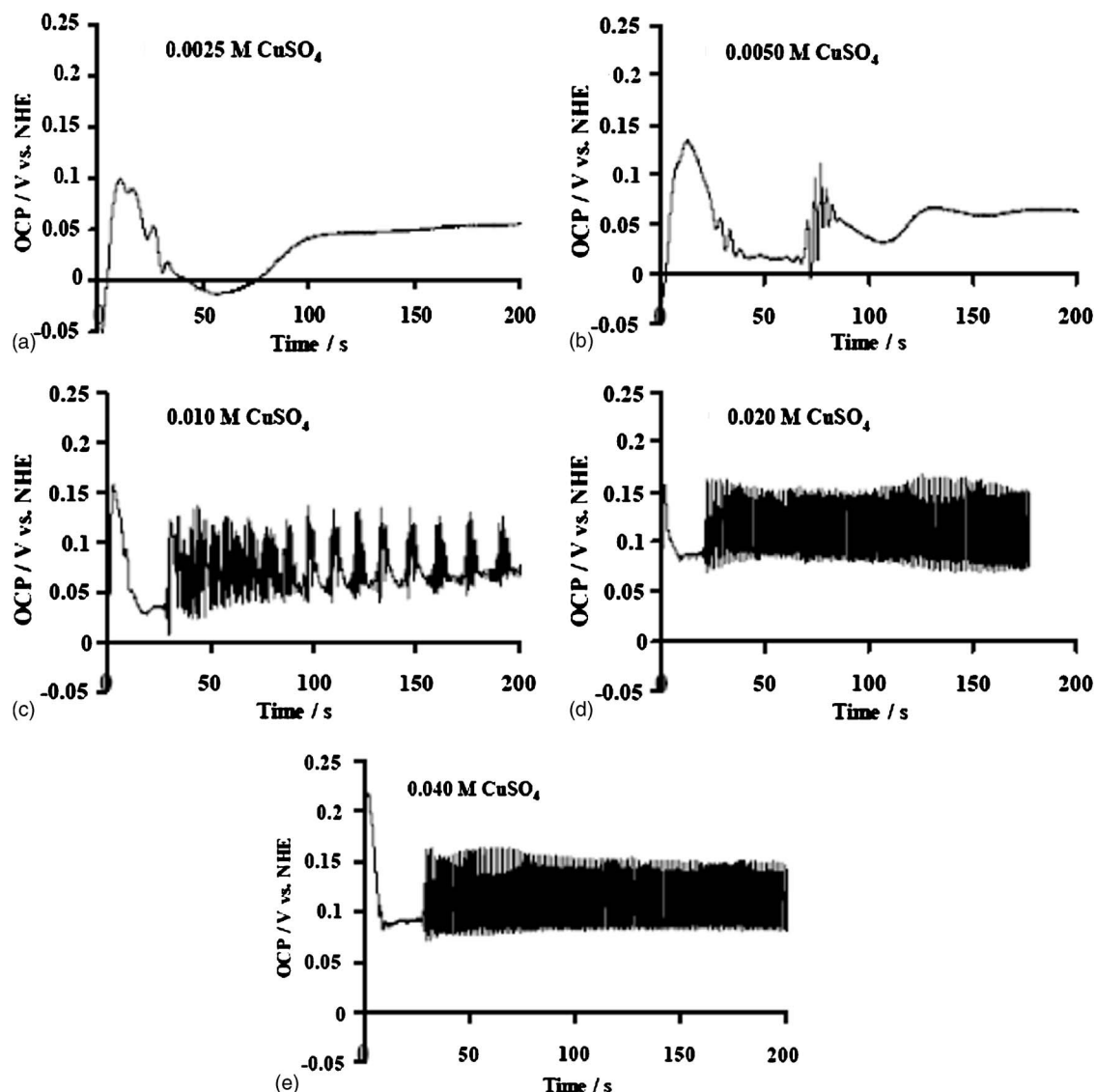


Figure 6. Effect of CuSO_4 concentration on time evolution of OCP values. $[\text{HF}] = 0.1 \text{ M}$; $[\text{CuSO}_4] =$ (a) 0.0025, (b) 0.005, (c) 0.01, (d) 0.02, and (e) 0.04 M; $\omega = 50 \text{ s}^{-1}$. OCP values increase as $[\text{CuSO}_4]$ increases, and oscillations are seen at longer times, particularly for high $[\text{CuSO}_4]$.

reflect the amount of Cu required to cover the entire Si surface without requiring subsequent nucleation and growth of Cu islands. Other features of the OCP profiles shown in Fig. 6 are the oscillations observed at long deposition times, which are particularly evident at higher CuSO_4 concentrations. These phenomena will be discussed in detail in a separate paper.

As shown above, Cu deposition occurs via sequential boundary layer diffusion and electrochemical reduction. Thus, the rate of the Cu^{2+} reduction half reaction can be found by rearranging Eq. 7 to solve for the deposition rate r . The kinetic rate constant k in Eq. 7 depends exponentially on the potential, leading to the following expression for the Cu^{2+} reduction rate^{8,42}

$$r_{\text{Cu}} = \frac{(0.62\nu^{-1/6}D_{\text{Cu}}^{2/3}\omega^{1/2})k_{\text{Cu}}^0 \exp\left[-\frac{\alpha F}{RT}(E - E_{\text{Cu}}^0)\right](\text{Cu}^{2+})}{0.62\nu^{-1/6}D_{\text{Cu}}^{2/3}\omega^{1/2} + k_{\text{Cu}}^0 \exp\left[-\frac{\alpha F}{RT}(E - E_{\text{Cu}}^0)\right]} \quad [8]$$

where k_{Cu}^0 is the standard Cu^{2+} reduction rate constant ($1.8 \times 10^{-5} \text{ cm s}^{-1}$), α is the transfer coefficient (0.46), F is Faraday's constant ($96,485 \text{ C mol}^{-1}$), R is the gas constant (8.314 J mol^{-1}

K^{-1}), T is the temperature (in Kelvin), and the other parameters are as defined in Eq. 6.⁴²

The effects of mass transfer were neglected in calculating Si dissolution rates, because diffusion of HF was found above not to limit Cu deposition rates (Fig. 4b). Si dissolution rate laws have been found previously for anodic oxidation of Si rotating disks by considering Si oxidation followed by dissolution of oxidized regions of the surface.⁴³ The rate of Si oxidation to Si^{2+} increases exponentially with increasing potential⁴⁴

$$r_{\text{Si,ox}} = k_{\text{Si}}^0 \theta_{\text{Si}} \exp\left[\frac{(1-\alpha)F}{RT}(E - E_{\text{Si}}^0)\right] \quad [9]$$

where θ_{Si} is the fraction of the Si surface covered by unoxidized Si, and the other terms are as defined above. Oxidized Si is then dissolved by parallel HF and HF_2^- pathways¹⁶

$$r_{\text{Si,diss}} = [k_{\text{HF}_2}(\text{HF}_2^-) + k_{\text{HF}}(\text{HF})](1 - \theta_{\text{Si}}) \quad [10]$$

Equations 9 and 10 can be combined by solving for θ_{Si} to determine the rate of Si oxidation and dissolution in terms of the potential and concentration of fluoride species⁴³

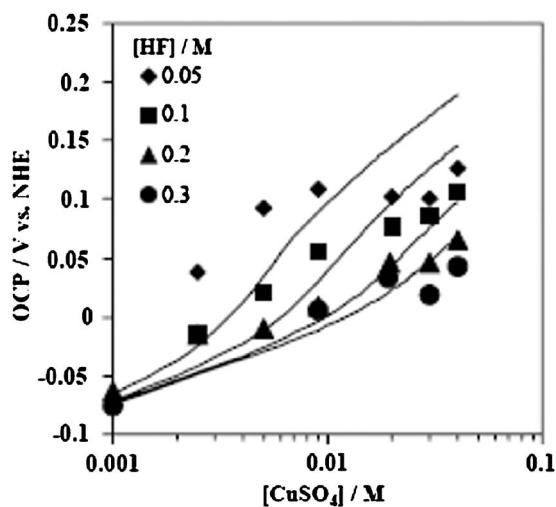


Figure 7. Effect of solution composition on OCP values. Solid lines represent OCP values calculated by setting the Cu^{2+} reduction rate in Eq. 8 equal to the Si oxidation rate in Eq. 11. $\omega = 50 \text{ s}^{-1}$.

$$r_{\text{Si}} = \frac{[k_{\text{HF}_2}(\text{HF}_2) + k_{\text{HF}}(\text{HF})]k_{\text{Si}}^0 \exp[(F/RT)(E - E_{\text{Si}}^0)]}{[k_{\text{HF}_2}(\text{HF}_2) + k_{\text{HF}}(\text{HF})] + k_{\text{Si}}^0 \exp[(F/RT)(E - E_{\text{Si}}^0)]} \quad [11]$$

In contrast with the Cu^{2+} reduction rates shown in Eq. 8, the rate of Si oxidation is not proportional to the concentration of fluoride species, which may explain why kinetic rates extracted from the Koutecky–Levich plots were not first order in $[\text{HF}]$ (Fig. 5b). When the second term in the denominator of Eq. 11 is much larger than the first, Si dissolution rates are independent of fluoride concentration and are limited entirely by the rate of Si oxidation. This situation arises for high HF concentrations and is consistent with deposition rates that became independent of HF concentration when HF was in large excess (Fig. 2). In contrast, if the second term in the denominator is much smaller than the first (low fluoride concentration), Si dissolution rates are proportional to the concentrations of fluoride species, as was seen for Cu deposition rates in dilute HF.

It can be seen in Eq. 8 and 11 that Cu reduction rates increase with decreasing E , while Si oxidation rates increase with increasing E . Thus, increasing the driving force for reduction relative to that for oxidation (through changes in solution composition, rotating speed, or parameter values) increases the OCP in order to keep oxidation and reduction rates equal. Conversely, increasing the driving force of oxidation relative to that for reduction causes the OCP to decrease. These trends are seen in the effects of solution composition (HF and CuSO_4 concentrations) on OCP values depicted in Fig. 7. The OCP values shown here are the constant (or nearly constant) values achieved after the maximum OCP values measured at short times. OCP values increased with increasing CuSO_4 concentration, as was shown in Fig. 6. In contrast, OCP values decreased with increasing HF concentration (Fig. 7) because of the consequent increase in the driving force for oxidation (Eq. 11). OCP values were not strongly affected when the HF concentration was increased above 0.2 M. This is consistent with deposition rate results, which showed the dissolution step no longer limited the rate of the Si half reaction.

Mixed-potential theory is used here to describe the effects of solution composition and rotating speed on Cu deposition rates and OCP values during deposition by solving for the potential E that equates the rates of Cu^{2+} reduction and Si oxidation (Eq. 8 and 11). The deposition rates calculated using this method are depicted as solid lines in Fig. 2, and the OCP estimates are compared to measured values in Fig. 7. These estimates agree well with rate data but

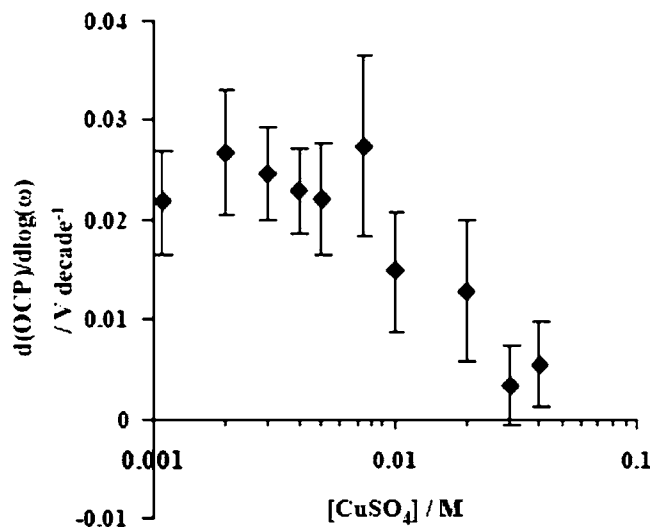


Figure 8. Effect of CuSO_4 concentration on the OCP change with rotating speed. The values are positive in all cases, indicating Cu^{2+} reduction is more mass-transfer limited than Si oxidation under these conditions. Lower values for high $[\text{CuSO}_4]$ indicate deposition rates become less limited by Cu^{2+} mass transfer. $[\text{HF}] = 0.1 \text{ M}$.

deviate significantly from OCP values, especially at low $[\text{HF}]/[\text{CuSO}_4]$ ratios, for which Cu deposition rates are limited by the rate of Si dissolution.

Figure 8 shows the effect of CuSO_4 concentrations of the slopes of OCP vs $\log \omega$ curves. The positive slopes indicate that the potential increased with increasing rotation speed at all concentrations, consistent with stronger mass transfer effects for Cu reduction than for Si oxidation rates. This is also consistent with deposition rate data (Fig. 4), which showed that gradients in Cu^{2+} concentration within the boundary layer are much greater than gradients in HF. OCP values increase at a nearly constant rate of 0.025 V per tenfold change in ω for CuSO_4 concentrations of $<0.005 \text{ M}$. The dependence of the potential on ω became weaker at higher CuSO_4 concentrations, indicating that Cu^{2+} concentration gradients become less pronounced and are ultimately negligible as CuSO_4 concentrations reach 0.04 M. The effect of mass transfer on deposition rates decreases for CuSO_4 concentrations of $>0.005 \text{ M}$, which corresponds to $[\text{HF}]/[\text{CuSO}_4]$ ratios below 20. This is the same ratio at which Si dissolution was found to influence deposition rates above (Fig. 2). Thus, these OCP measurements are consistent with deposition rates described above and indicate the change in the rate-limiting step as the solution composition is varied.

Effect of rate-limiting process on film structure.— The surfaces of Cu films were studied using AFM to determine how film morphology was influenced by the various processes controlling film growth. AFM scans of the surfaces of Cu films deposited in solutions containing 0.20 M HF and 0.0050 M CuSO_4 are shown in Fig. 9. Cu forms nuclei ~ 100 to 200 nm diam on Si, and the surface is nearly completely covered by Cu within 30 s. Cu domains tend to be oblate, with heights of ~ 30 to 50 nm. The size of these domains does not appear to increase with deposition time, and the Cu films formed are smooth (rms roughness $\sim 10 \text{ nm}$) after 240 s of deposition, when such films are $\sim 200 \text{ nm}$ thick.

Much rougher Cu films formed at lower HF concentrations (0.05 M) (Fig. 10). Nucleation rates are lower than at higher HF concentrations, and a significant fraction of the Si surface remains bare after 30 s. These lower nucleation rates are consistent with the lower deposition rates measured in more dilute HF solutions (Fig. 2). Cu films become much rougher as time progresses, and the grains appear to grow with time. Cross-sectional images of the films show that distinct particles as tall as 200 nm formed at low HF

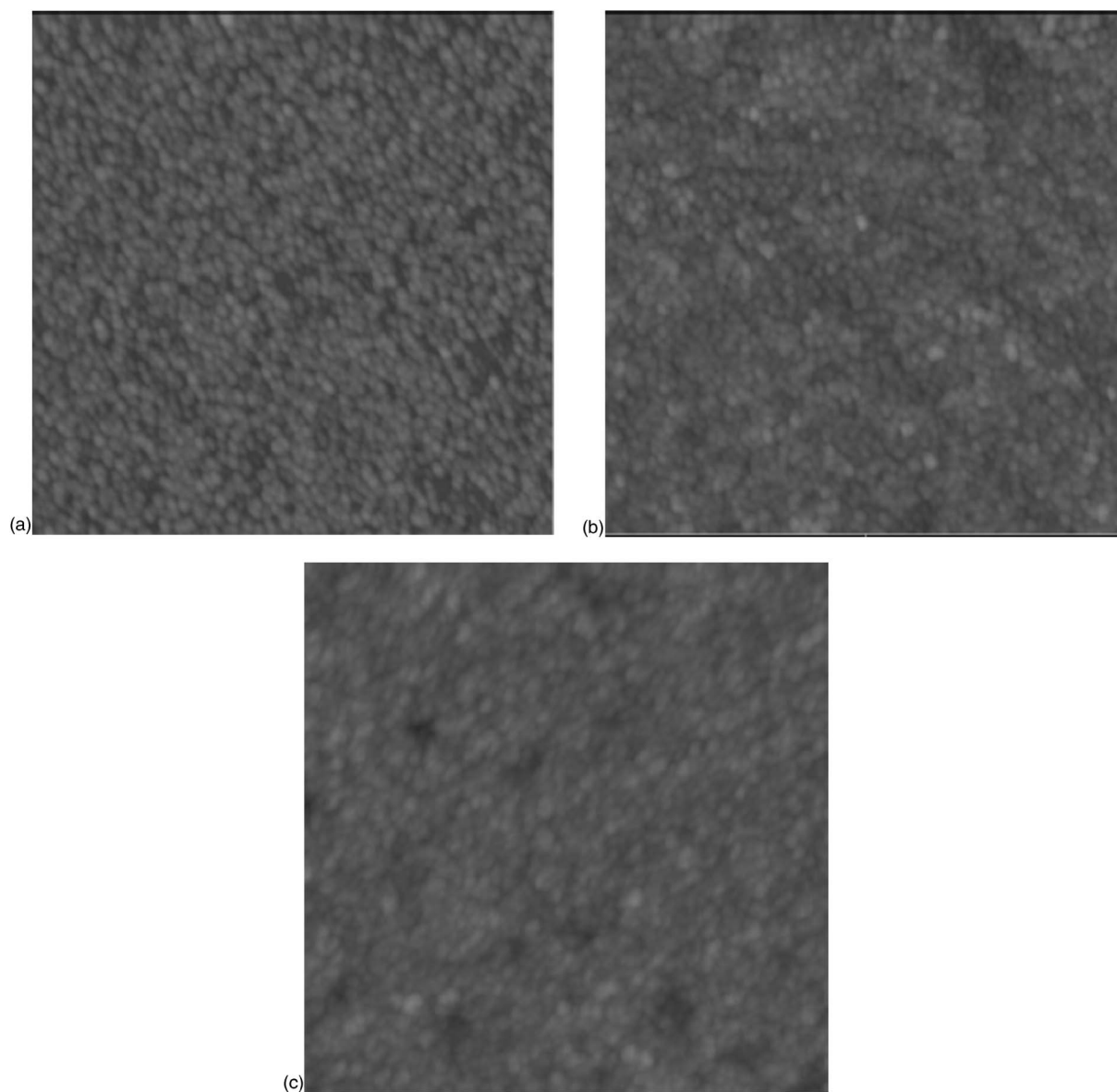


Figure 9. $5 \times 5 \mu\text{m}$ AFM scans of Cu films deposited for (a) 30, (b) 120, and (c) 240 s. $[\text{HF}] = 0.2 \text{ M}$, $[\text{CuSO}_4] = 0.005 \text{ M}$, $\omega = 50 \text{ s}^{-1}$. The vertical scale in all images is 200 nm. The average film thicknesses are (a) 45 nm, (b) 140 nm, and (c) 210 nm.

concentrations, while continuous films formed at high HF concentrations. These trends and structures resemble those reported for deposition of Ag on Ge, for which nanoparticles were formed on previously oxidized Ge surfaces and continuous films were formed on reduced surfaces.²³ These authors proposed that individual particles formed on oxidized surfaces because electron-transfer (and thus reduction) rates were greater at the metal particles than on the Ge surface. Similarly, Si surfaces are expected to be more oxidized at lower HF concentrations because of a decreased rate of oxide dissolution, leading to preferential deposition on Cu metal particles.

The results above indicate Cu surface properties can be modified by varying the relative rates of Cu^{2+} reduction and Si dissolution. Figure 11 depicts the effect of the $[\text{HF}]/[\text{CuSO}_4]$ ratio on film roughness. The roughness decreases as the $[\text{HF}]/[\text{CuSO}_4]$ ratio increases over the entire range studied. These results are independent of deposition rate, indicating both the rate and the roughness can be tailored for the desired application and processing requirements.

Conclusions

The effects of Cu^{2+} reduction and Si dissolution on the rate of Cu deposition onto Si and the resulting film properties were studied. Either Cu^{2+} reduction or Si dissolution is found to limit the rate, depending on the solution composition. Deposition rates are limited by Cu^{2+} reduction only when the $[\text{HF}]/[\text{CuSO}_4]$ is greater than ~ 20 , and rates are primarily limited by Si dissolution when the $[\text{HF}]/[\text{CuSO}_4]$ ratio is less than ~ 10 . Mass transfer of Cu^{2+} ions was found to limit deposition rates, but diffusion of HF did not. These results were also supported by OCP measurements, which indicated Cu^{2+} reduction was more limited by mass transfer than Si oxidation and dissolution. OCP measurements supported kinetic data that suggested HF_2^- was the primary Si etchant. Mixed potential theory was used to predict deposition rates and OCP values in reasonable agreement with experimental results. The relative rates of Si dissolution and Cu deposition were also found to strongly affect the morphology of Cu films. Much rougher films form when Si disso-

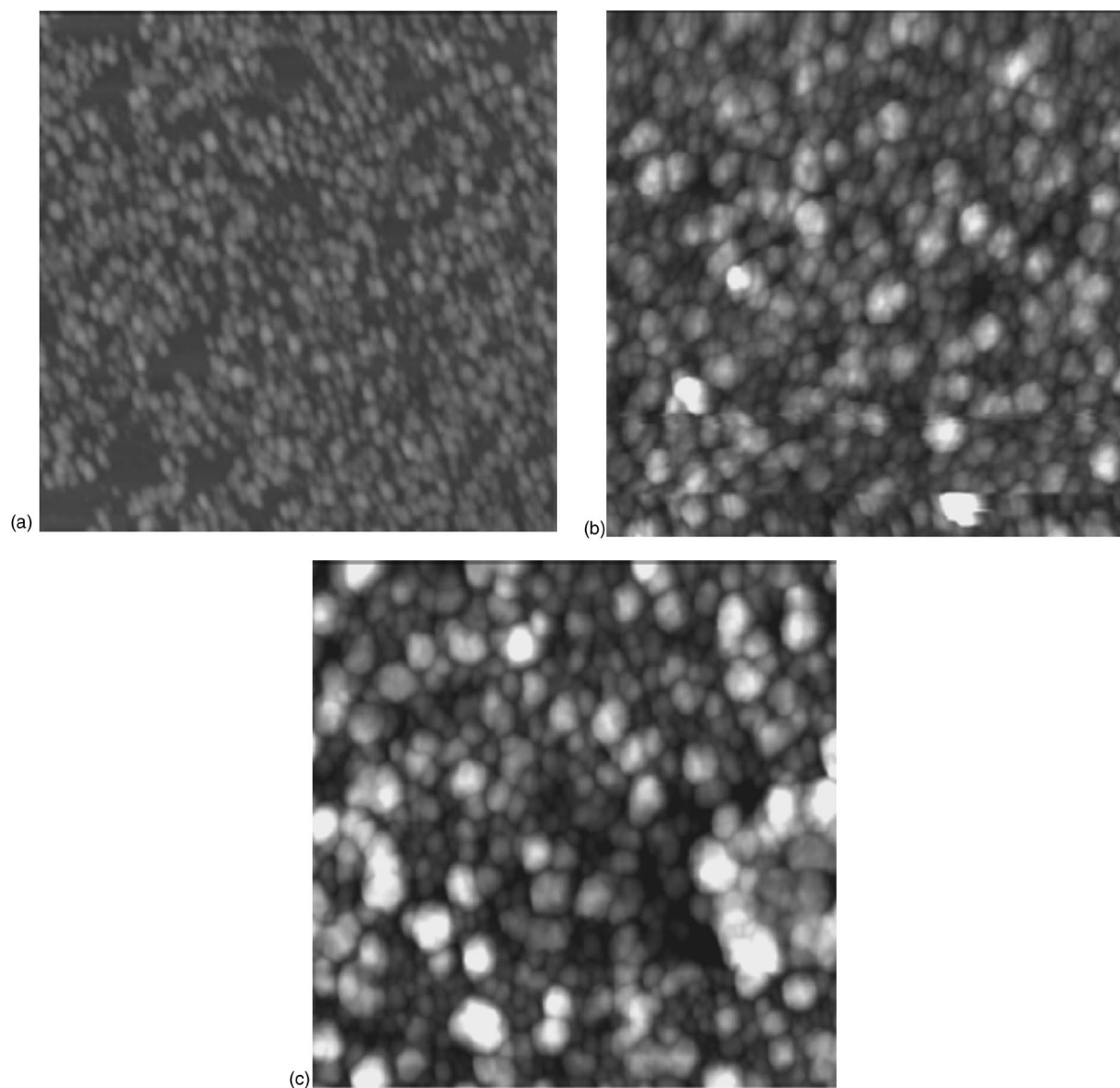


Figure 10. $5 \times 5 \mu\text{m}$ AFM scans of Cu films deposited for (a) 30, (b) 120, and (c) 240 s. $[\text{HF}] = 0.05 \text{ M}$, $[\text{CuSO}_4] = 0.005 \text{ M}$, $\omega = 50 \text{ s}^{-1}$. The vertical scale in all images is 200 nm. The average film thicknesses are (a) 35 nm, (b) 70 nm, and (c) 130 nm.

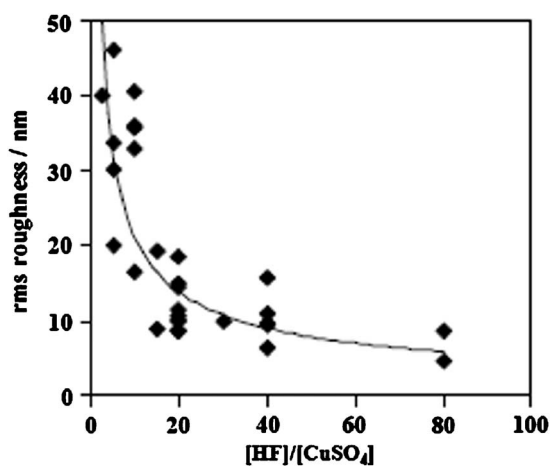


Figure 11. Effect of $[\text{HF}]/[\text{CuSO}_4]$ ratio on the rms roughness of Cu films. Rough films form when Si dissolution limits the rate, and smooth films form when Cu^{2+} reduction limits the rate. Film thickness = 80 nm. The solid line is a guide for the eyes.

lution limits the rate. These results show that film roughness and deposition rates can be modified independently according to the properties desired for the intended application.

Acknowledgments

We acknowledge Professor Elton Cairns for the use of the RDE. C. P. daRosa thanks the National Science Foundation and Chevron for fellowship support. This research was funded by the Committee on Research of the University of California, at Berkeley and the National Science Foundation.

University of California assisted in meeting the publication costs of this article.

References

1. C. Carraro, R. Maboudian, and L. Magagnin, *Surf. Sci. Rep.*, **62**, 499 (2007).
2. L. Magagnin, R. Maboudian, and C. Carraro, *Electrochem. Solid-State Lett.*, **4**, C5 (2001).
3. C. H. Wang, D. C. Sun, and X. H. Xia, *Nanotechnology*, **17**, 651 (2006).
4. H. H. Lin, J. Mock, D. Smith, T. Gao, and M. J. Sailor, *J. Phys. Chem. B*, **108**, 11654 (2004).
5. M. Green and F. M. Liu, *J. Phys. Chem. B*, **107**, 13015 (2003).
6. J. Zhang, F. H. B. Lima, M. H. Shao, K. Sasaki, J. X. Wang, J. Hanson, and R. R.

- Adzic, *J. Phys. Chem. B*, **109**, 22701 (2005).
7. A. T. Carvalho, A. P. Nascimento, L. M. Silva, M. L. P. Silva, J. C. Madaleno, and L. Pereira, *Mater. Sci. Forum*, **514-516**, 1328 (2006).
 8. A. J. Bard and L. R. Faulkner, *Electrochemical Methods: Fundamentals and Applications*, Wiley, Hoboken, NJ (2001).
 9. A. T. Kuhn and C. L. Rise, in *Standard Potentials in Aqueous Solutions*, A. J. Bard, R. Parsons, and J. Jordan, Editors, p. 189, Marcel Dekker, New York (1985).
 10. M. K. Lee, H. D. Wang, and J. J. Wang, *Solid-State Electron.*, **41**, 695 (1997).
 11. L. Torcheux, A. Mayeux, and M. Chemla, *J. Electrochem. Soc.*, **142**, 2037 (1995).
 12. K. G. Mishra and R. K. Paramguru, *J. Electrochem. Soc.*, **147**, 3302 (2000).
 13. N. Demirkiran, A. Ekmekyapar, A. Kunkul, and A. Baysar, *Int. J. Min. Process.*, **82**, 80 (2007).
 14. R. M. Nadkarni and M. E. Wadsworth, *Trans. Metall. Soc. AIME*, **239**, 1066 (1967).
 15. W. C. Ye, Y. L. Chang, C. L. Ma, B. Y. Jia, G. Y. Cao, and C. M. Wang, *Appl. Surf. Sci.*, **253**, 3419 (2007).
 16. J. S. Judge, *J. Electrochem. Soc.*, **118**, 1772 (1971).
 17. L. Koker and K. W. Kolasinski, *J. Phys. Chem. B*, **105**, 3864 (2001).
 18. K. W. Kolasinski, *Phys. Chem. Chem. Phys.*, **5**, 1270 (2003).
 19. K. W. Kolasinski, *Curr. Opin. Solid State Mater. Sci.*, **9**, 73 (2005).
 20. M. Nahidi and K. W. Kolasinski, *J. Electrochem. Soc.*, **153**, C19 (2006).
 21. R. Srinivasan and I. I. Suni, *J. Electrochem. Soc.*, **146**, 570 (1999).
 22. L. A. Nagahara, T. Ohmori, K. Hashimoto, and A. Fujishima, *J. Electroanal. Chem.*, **333**, 363 (1992).
 23. J. Yang and P. R. Griffiths, *Anal. Bioanal. Chem.*, **388**, 109 (2007).
 24. X. Zhang, F. Ren, M. S. Goorsky, and K. N. Tu, *Surf. Coat. Technol.*, **201**, 2724 (2006).
 25. C. P. daRosa, E. Iglesia, and R. Maboudian, *J. Electrochem. Soc.*, **155**, D234 (2008).
 26. S. G. dos Santos, L. F. O. Martins, P. C. T. D'Ajello, A. A. Pasa, and C. M. Hasenack, *Microelectron. Eng.*, **33**, 59 (1997).
 27. E. Hsu, H. G. Parks, R. Craigin, S. Tomooka, J. S. Ramberg, and R. K. Lowry, *J. Electrochem. Soc.*, **139**, 3659 (1992).
 28. M. J. Eddowes, *J. Electroanal. Chem. Interfacial Electrochem.*, **280**, 297 (1990).
 29. J. N. Chazalviel, M. Etman, and F. Ozanam, *J. Electroanal. Chem. Interfacial Electrochem.*, **297**, 533 (1991).
 30. M. Etman, M. Neumannspallart, J. N. Chazalviel, and F. Ozanam, *J. Electroanal. Chem. Interfacial Electrochem.*, **301**, 259 (1991).
 31. H. H. Hassan, J. L. Sculfort, M. Etman, F. Ozanam, and J. N. Chazalviel, *J. Electroanal. Chem.*, **380**, 55 (1995).
 32. H. Kikuyama, M. Waki, M. Miyashita, T. Yabune, N. Miki, J. Takano, and T. Ohmi, *J. Electrochem. Soc.*, **141**, 366 (1994).
 33. X. G. Zhang, *Electrochemistry of Silicon and Its Oxide*, p. 133, Plenum Press, New York (2001).
 34. J. G. A. Brito-Neto, S. Araki, and M. Hayase, *J. Electrochem. Soc.*, **153**, C741 (2006).
 35. K. W. Kolasinski, *J. Electrochem. Soc.*, **152**, J99 (2005).
 36. R. Braddy, P. T. McTigue, and B. Verity, *J. Fluorine Chem.*, **66**, 63 (1994).
 37. T. Nagai, S. Nakanishi, Y. Mukouyama, Y. H. Ogata, and Y. Nakato, *Chaos*, **16**, 037106 (2006).
 38. *CRC Handbook of Chemistry and Physics, Internet Version 2007*, Taylor and Francis, Boca Raton (2007).
 39. V. G. Levich, *Physicochemical Hydrodynamics*, Prentice-Hall, Englewood Cliffs, NJ (1962).
 40. G. P. Power and I. M. Ritchie, *Aust. J. Chem.*, **29**, 699 (1976).
 41. G. P. Power and I. M. Ritchie, *Electrochim. Acta*, **26**, 1073 (1981).
 42. J. T. Hinatsu and F. R. Foulkes, *Can. J. Chem.*, **69**, 571 (1991).
 43. J. van den Meerakker and M. R. L. Mellier, *J. Electrochem. Soc.*, **148**, G166 (2001).
 44. P. C. Searson and X. G. Zhang, *J. Electrochem. Soc.*, **137**, 2539 (1990).